Tellus (1987), *39A*, 474–491

Error growth and predictability in operational ECMWF forecasts

By AMNON DALCHER* and EUGENIA KALNAY, *Laboratory for Atmospheres, Code 611, NASA/Goddard Space Flight Center, Greenbelt, Maryland, USA*

(Manuscript received 21 February; in final form 29 December 1986)

ABSTRACT

We study the forecast error growth in the 100-day ECMWF data set of 10-day forecasts previously utilized by Lorenz, separating the square of the error into systematic and random components. The random error variance is approximately equally distributed among all zonal wavenumbers m corresponding to the same total wavenumber n. Therefore, we combine the random error variance for all zonal wavenumbers and study its dependence on total (2-dimensional) wavenumber rather than on zonal wavenumber.

We extend the Lorenz model for global r.m.s. error growth by *including the effect of errors associated with deficiencies in the forecast model*, and apply this new parameterization to the error variance of 10-day ECMWF operational forecasts obtaining an excellent fit. We point out that the commonly used parameter "doubling time of small errors" is *not* a good measure of error growth because it has to be determined by extrapolation to small errors and it is very sensitive to the method of extrapolation. On the other hand, the error growth at finite times is a better measure because it is well defined by the data.

The results of the error fit to each total wavenumber n are the basis for the main conclusions of the paper. In the northern hemisphere winter data set, the error growth rate α increases almost monotonically with wavenumber, from about 0.3 day^{-1} at long waves to about 0.45 day^{-1} at medium and short waves. The saturation error variance V_∞ is about 30% larger than the error variance at day 10 for long waves, which have not yet reached saturation. The scaled source of external error S/V_∞ (due to model deficiencies) varies from about 3% day^{-1} at long waves to about 20% day^{-1} at short waves. This increase of relative model error may be due to the second-order finite differences used in the ECMWF model during 1980/1981.

Finally, we estimate *the theoretical limit of dynamical predictability as a function of total wavenumber n*. We define it as the time at which the error variance reaches 95% of the saturation value. This time *decreases monotonically with n*. In the winter, waves $n \leqslant 10$ have not reached saturation at 10 days. In a perfect model with error growth similar to the present model, the predictability limit would be extended by about a week. In the summer, error growth rates and model deficiencies are larger than in winter, and the limit of predictability is close to 10 days even for long waves.

1. Introduction

The estimation of the rate of growth of forecast errors has been the central objective of several classical studies on atmospheric predictability (Lorenz, 1965; Charney et al., 1966; Smagorinsky, 1969, and others). These studies were all performed using the "identical twin" technique: they measured how fast two model integrations, started from very close initial conditions and computed using the same atmospheric model, departed from each other. From these experiments, estimates of the doubling time for small differences were obtained, and it was concluded that the theoretical limit of deterministic atmospheric predictability was of the order of two weeks. Because of the implicit

* M/A COM Sigma Data Corp. at NASA/Laboratory for Atmospheres, USA.

assumption of a perfect model, the identical-twin experiments only provided an upper limit of atmospheric predictability.

The most recent and detailed study of this type has been that of Lorenz (1982) who used as a data base 100 consecutive ten-day operational forecasts from the European Centre for Medium Range Forecasting. His study was also of an identical-twin type, because he computed the average growth of the difference between two model forecasts verifying on the same day. Lorenz (1982) showed that the growth of the r.m.s. difference E in 500 mb heights between two forecasts with the same model is reasonably well parameterized by the equation

$$\mathrm{d}E/\mathrm{d}t = aE(E_\infty - E). \tag{1.1}$$

This equation allows for exponential growth of small differences with a growth rate given by $(a \cdot E_\infty)$ as well as for saturation at long times, when 2 forecasts verifying on the same day have ceased to resemble each other any more than 2 randomly chosen states of the atmosphere. The saturation value obtained by Lorenz was $E_\infty \sim 110$ m, and the exponential growth rate corresponded to a doubling time for small errors of only 2.4 days, considerably less than previous estimates.

Lorenz also pointed out that the same data set provides a lower bound for atmospheric predictability, simply given by the actual skill of the ECMWF forecasts verified against the atmospheric analysis. By extrapolating the curve representing the growth of the difference between two forecasts (eq. 1.1), he concluded that with a perfect model, 14-day forecasts could be as good as the present 8-day forecasts, even if the same errors were made during the first forecast day.

Boer (1984) has recently performed an analysis of the error growth in the 3-day operational forecasts of the Canadian Meteorological Centre. His approach was to obtain a forecast equation for the error enstrophy and estimate the components of the error budget as a function of n, the order of the associated Legendre polyomials, equivalent to a 2-dimensional wavenumber on the sphere. Savijärvi (1984) studied the spectral structure of both analysis and forecasts using the same ECMWF data set as Lorenz.

In this paper we extend Lorenz's parameterization (1.1) by including the effect of growth of errors due to model deficiencies. In this way we are able to fit the *real* forecast error growth and determine the scale dependence of the derived parameters (rate of error growth, external error source due to model errors, error saturation level and the limit of dynamical predictability). One application of this work is the determination of optimal weights to be used in applying the Lagged Average Forecasting (LAF) technique (Hoffman and Kalnay, 1983, 1984) to the ECMWF 10-day forecasts (Dalcher et al., 1985).

In Section 2, we analyze the nature of ECMWF systematic and random forecast errors in the spherical harmonics wavenumber domain. Section 3 contains the new parameterization and its application to global errors and Section 4 presents the wavenumber dependence of error growth.

2. Systematic and random mean-square forecast errors

The forecast data set that we use is the same previously studied by Lorenz (1982), Wallace et al. (1983) and Savijärvi (1984). For each of 100 consecutive days, it contains an analysis and 10 forecasts started from the analysis 1 day earlier, 2 days earlier, ..., 10 days earlier, all verifying on the same day. Each 500 mb geopotential height field is defined by the coefficients of its spherical harmonic expansion, with a triangular truncation T40, and a total of $41 \times 41 = 1681$ coefficients. There are two 100-day data sets available, one for the winter of 1980/1981 which starts on 1 December 1980, and one for the summer of 1981, starting on 1 June 1981. Although our analysis is made globally, we refer to the results as "winter" or "summer" according to the northern hemisphere season, since the northern hemisphere dominates the global variations.

We define the error as the difference between a forecast field ϕ_f and the analysis ϕ_v corresponding to the verification time. Because of the advantages that the additive property of variances brings, we choose to work with the square of the errors rather than the r.m.s. errors considered by Lorenz (1982).

We separate the mean square error in the systematic and non-systematic or random component i.e.,

$$\overline{(\phi_f - \phi_v)^2} = (\bar{\phi}_f - \bar{\phi}_v)^2 + \overline{(\phi_f' - \phi_v')^2} \tag{2.1}$$

when the overbar represents the average over 100 days and primes the departures from this average. Although this definition of systematic error is convenient for this data set, it is not as useful in an operational context. F. Hughes (NMC, personal communication) has suggested that systematic error be defined by a running average over the 30 days previous to the operational forecast. Most of the paper will be devoted to the last term in (2.1), which we denote as error variance, non-systematic error squared or random error squared.

We first consider the spectral distribution of systematic and random errors, using the real representation of spherical harmonics Y_n^m. The harmonics are scaled so that the integral of their squared value over the sphere is equal to 4π – the area of the unit sphere. In order to compute squared errors, we sum for each wavelength m, n ($m > 0$), the square of the $\cos(m\lambda)$ and $\sin(m\lambda)$ terms. The values corresponding to zonal wavenumber $m = 0$ in Figs. 1 and 3 are multiplied by a factor of 2, in order to emphasize equipartition of energy between modes, since for

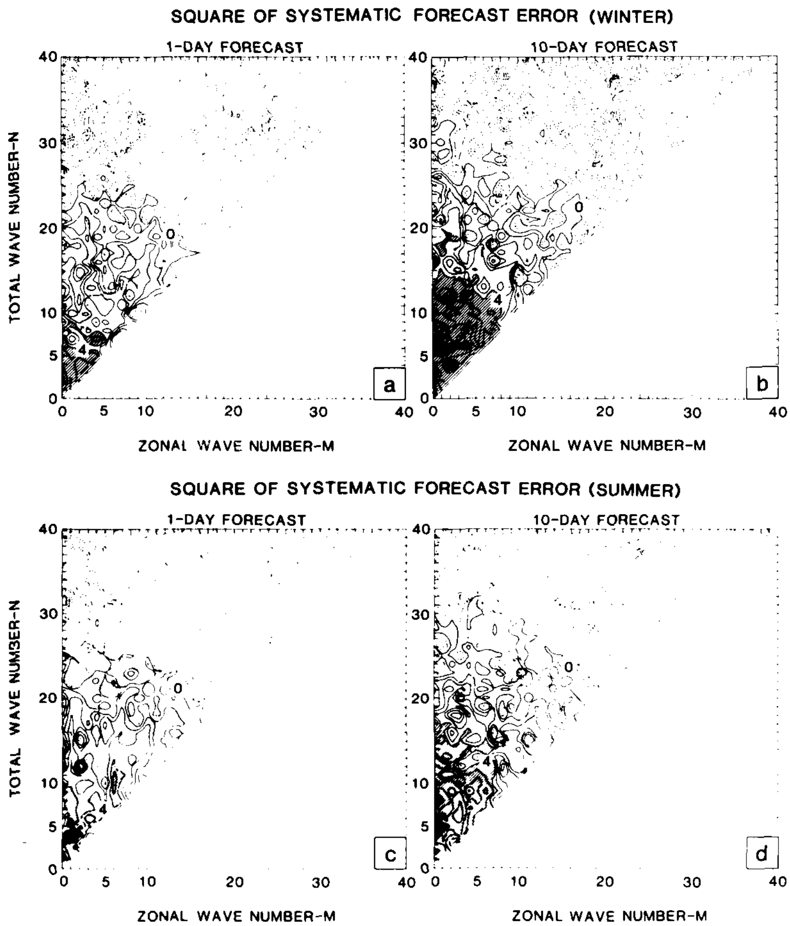

Fig. 1. Logarithm of the systematic (mean) error squared as a function of m and n the zonal and total spherical harmonic wavenumber. Contour interval = 1. Errors larger than $C = 8$ (corresponding to a height error of $e^2 \sim (5.6\ \mathrm{m})^2$) are shaded, and values larger than $C = 4$ (height error of $e^2 = (0.75\ \mathrm{m})^2$) are hatched (contour interval = 1): (a) winter 1-day forecast; (b) winter 10-day forecast; (c) summer 1-day forecast; (d) summer 10-day forecast.

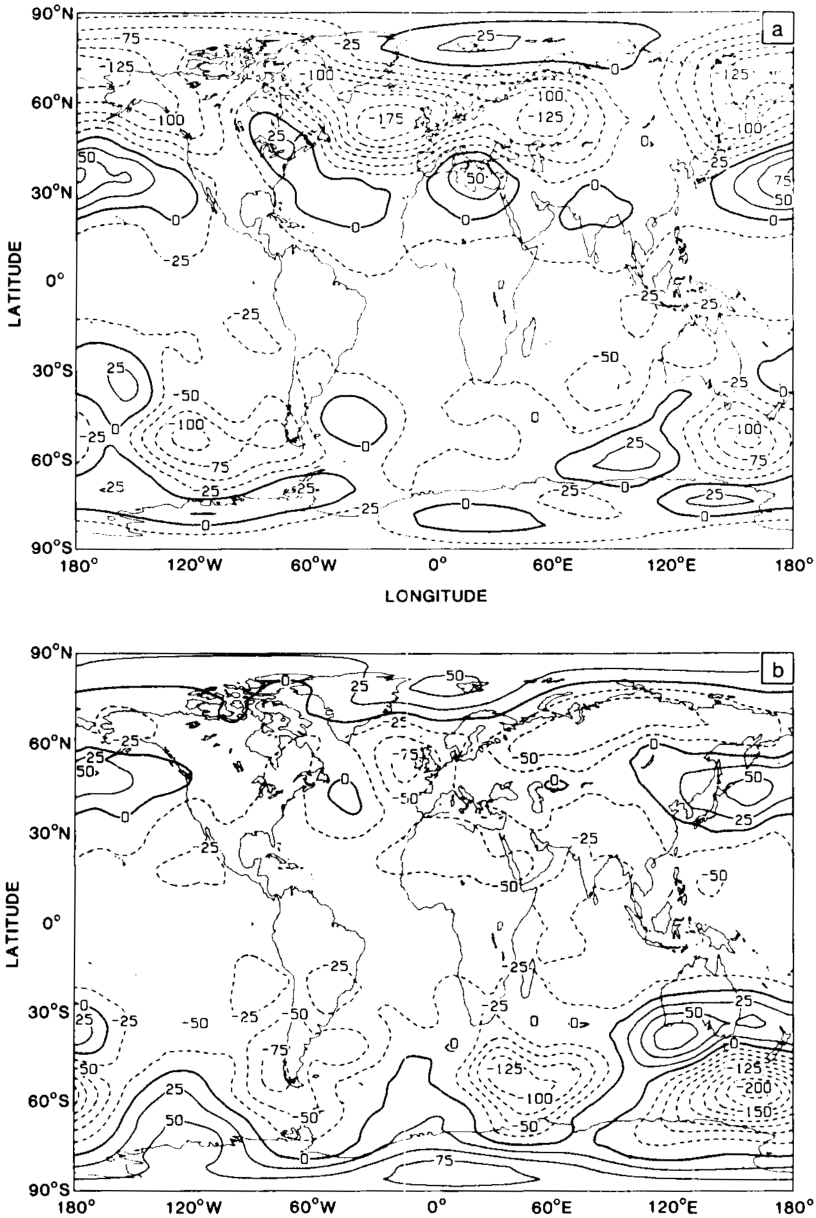

Fig. 2. Systematic 10-day 500 mb height forecast error: (a) winter; (b) summer. (Contour interval = 10 m.)

$m = 0$ there is only a cosine term, whereas modes with $m > 0$ have contributions from both the cosine and the sine terms.

Fig. 1 shows the *systematic* error squared as a function of m and n. In the winter (Figs. 1a, 1b) it is evident that at all times the systematic error growth is dominated by a few wave components, such as Y_0^0 which grows due to an overall cooling of the model, and Y_6^0, which corresponds to a banded structure of *meridional wavenumber* 3

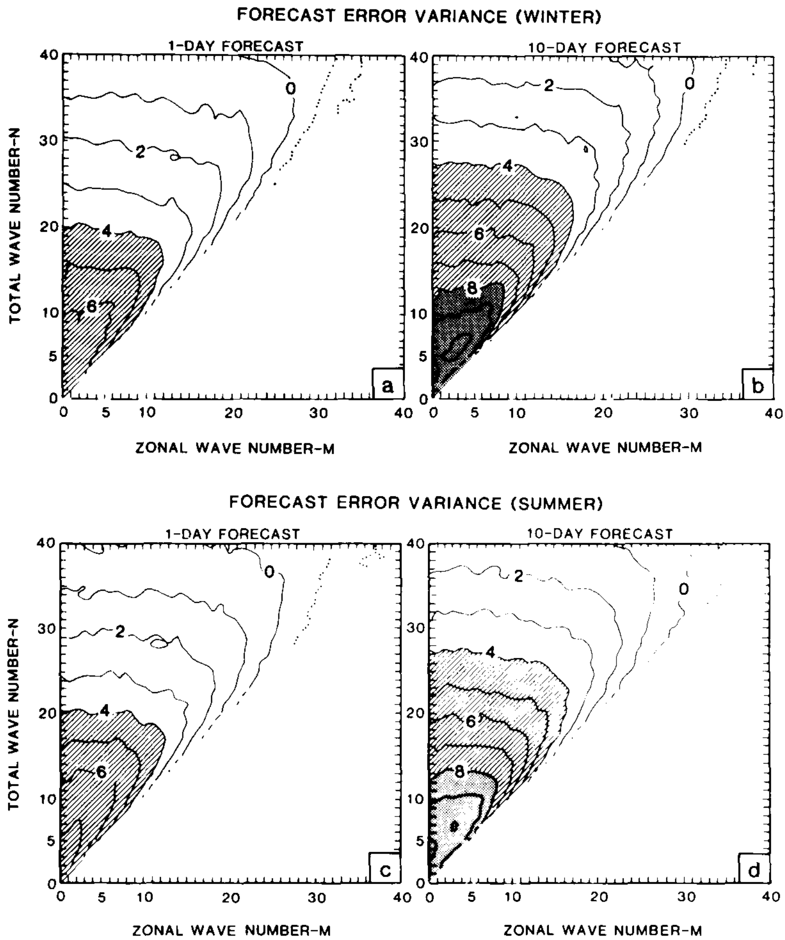

Fig. 3. Same as Fig. 1 but for the random error variance.

somewhat apparent in the systematic 10-day error map (Fig. 2a). The mean analysis energy distribution (not shown) is also dominated by a few long wave components. The summer systematic error (Figs. 1c, 1d) is also dominated by a few low wave number components, especially those with $m = 0$, indicating a strongly zonal character of the summer systematic error (Fig. 2b).

On the other hand, when we observe the wavenumber distribution of the error variance, a very different picture emerges (Fig. 3). For both the analyses and the forecasts (not shown) there is an approximate equipartition of energy between all the zonal wavenumbers m corresponding to the same total wavenumber n. This remarkable fact was also noticed by Savijärvi (1984) using the same data set, and by Boer (1984), who analysed Canadian 3-day forecasts. It should be noted however, that for a given total wavenumber n the energy tends to decrease rapidly as $m \sim n$, i.e., as the meridional wavenumber goes to zero. This can be attributed to the fact that for low values of the meridional wavenumber $n - m$, the Legendre polynomials decrease quickly away from the tropics. As pointed out by Savijärvi (1984), this, combined with the geostrophic constraint, imposes small amplitudes in the geopotential heights of these modes.

These observations show that systematic and random errrors have a fundamentally different nature, and therefore should be considered separately. The equipartition of energy between zonal modes corresponding to the same 2-dimensional wavenumber n suggests that in the study of random errors, we should focus on their 2-D total wavenumber dependence, rather than on the zonal wavenumber as has been generally done so far (e.g. Bengtsson, 1985; Shukla, 1981). This has two added advantages: it reduces the number of degrees of freedom to be considered, and it emphasizes the dependence of random errors on the 2-D scale.

Fig. 4a, b compare the global value of the total mean squared error (systematic plus random) with the forecast error variance. It is clear that the systematic error (shaded) constitutes about 20% of the total error energy both in the winter and in the summer. The quasi-horizontal line in Fig. 5 represents the analysis and forecast variance about the mean, indicating that in the winter (Fig. 4a) the model simulates well the total atmospheric variability, although in the summer this is less true (Fig. 4b).

Fig. 5 shows the distribution of the logarithm of height variance as a function of the logarithm of the total wave number. (In the presentation of results corresponding to the single wave number n, we add the variances or mean square of all components Y_n^m with the same n.) For each season the analysis and the 1 to 10-day forecast have a very similar structure.

For the winter we show the analysis field (Fig. 5a), and the 10-day forecast field (Fig. 5b). As in all the winter fields their spectra have an absolute maximum at total wave number 5, are almost flat in the range 5 - 8, and in the range 15 - 40 decay almost linearly. The figures also show a straight line fitted to the data in the range $20 \leqslant n \leqslant 29$ which is barely distinguishable from the curve. Its slope is -5.1 for the analysis and -4.9 for the 10-day forecast. These slopes are consistent with a -5 slope predicted for the inertial range by geostrophic turbulence theory. The spectra for the summer are fairly similar to the winter spectra. Again we show the analysis field (Fig. 5c) and the 10-day forecast field (Fig. 5d). The location of the global maximum shifts to $n = 7$, the spectra are fairly flat in the range 5 - 9, the slopes of the fitted lines are -5.3 for the analysis and -4.9 for the 10-day forecast. In both summer and winter there is a local minimum of the spectra for $n = 2$.

Fig. 6 presents the growth of the square of the systematic error as a function of forecast time for wavenumbers between $n = 0$ and $n = 9$. In this and in the following figures dimensional units are presented on the right and scaled nondimensional units on the left. In the winter (Fig. 6a, b), the only two dominant modes are again $n = 0$ and $n = 6$, which are still growing at the end of the 10-day forecast period. The other components are smaller in magnitude and have a tendency to saturate faster. In the summer (Fig. 6c, d), the largest modes, $n = 0$, 5 and 6 are also still growing at the end of the period.

The corresponding result for the error variance (square of the non-systematic error) for $n = 0$ to

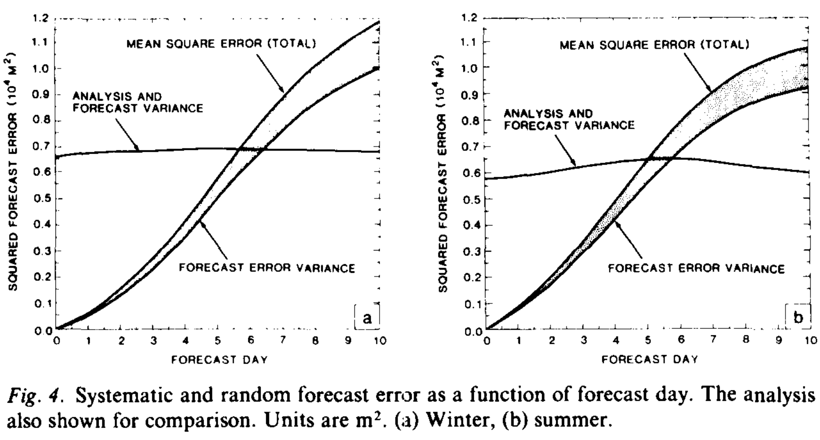

Fig. 4. Systematic and random forecast error as a function of forecast day. The analysis and forecast variance are also shown for comparison. Units are m^2. (a) Winter, (b) summer.

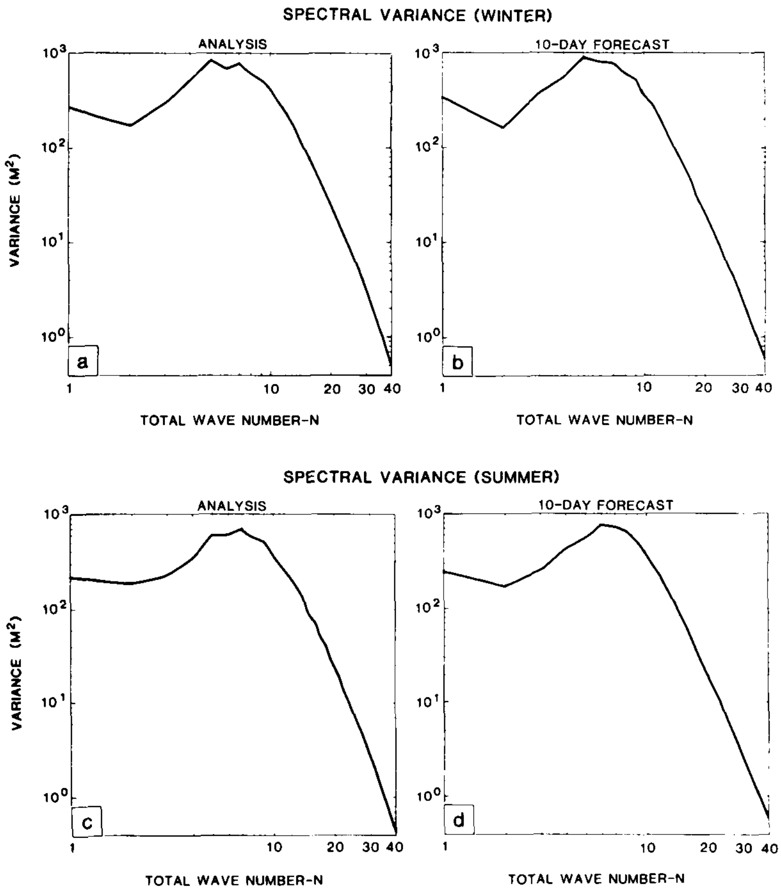

Fig. 5. Logarithm of the forecast or analysis variance as a function of log of the total wave number with fitted straight line: (a) winter analysis; (b) winter 10-day forecast; (c) summer analysis; (d) summer 10-day forecast.

$n = 19$ is shown in Figs. 7 and 8. Several observations stand out: (a) the forecast error variance grows with wavenumber from $n = 0$ to $n = 7$, where it acquires its maximum amplitude. From $n = 8$ to $n = 15$ it decreases monotonically, and beyond $n = 16$, it is quite small; (b) forecast error saturation, when no further error growth is observed, is reached at longer times for longer wavelengths. Waves with $n < 5$ have error variances which are still growing strongly at the end of the 10-day forecast period, waves with $n \approx 10$ start to reach saturation at about or after 10 days, and saturation is reached at earlier times for larger wavenumbers. Beyond $n = 15$, wave error reaches saturation within the first five days. These observations are true for both winter and summer, although there is a tendency to saturate faster in the summer (compare, for example, wavenumber $n = 7$ in Figs. 7 and 8). The fact that error saturation takes place at later times for long waves is in basic agreement with the results of Shukla (1981), although he performed his analysis at one latitude circle, and using only zonal wavenumbers.

3. Parameterization of the forecast error growth

As indicated in the introduction, Lorenz (1982) showed that the internal r.m.s. forecast error growth can be parameterized reasonably well by

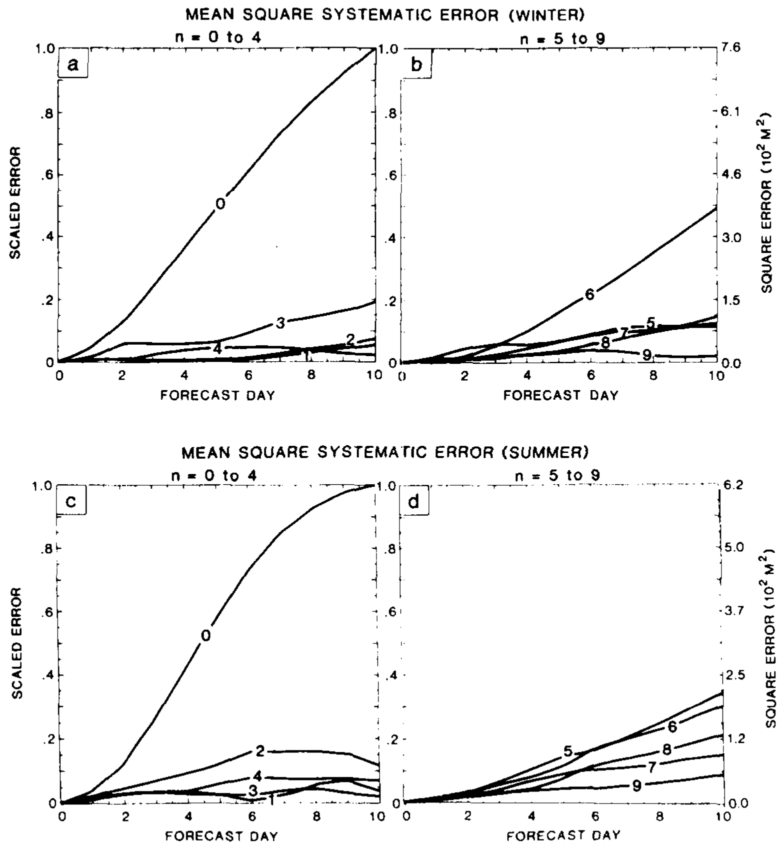

Fig. 6. Individual growth of the mean squared systematic error for waves with total wavenumber $n = 0, 1, \ldots 9$. Winter (a) $n = 0, \ldots 4$, (b) $n = 5, \ldots 9$. Summer (c) $n = 0, \ldots 4$, (d) $n = 5, \ldots 9$.

eq. (1.1). However this parameterization is not suitable for real forecast error growth (cf. his Fig. 1), because by not allowing for errors due to model deficiencies it is valid only for "identical twin" comparisons. Furthermore, no scale distinction is made in this parameterization.

Leith (1978, 1982) has suggested that the deficiencies of a model which make it different from the real atmosphere, are an "external" source of error growth which must be included if we want to represent real forecast error growth. He also suggested that it is preferable to model error variances V rather than r.m.s. errors E. However, his suggested parameterization

$$dV/dt = \alpha V + S \tag{3.1}$$

is only good for short times since it does not allow for saturation.

In this work, we decided to parameterize the error variance growth by including both an external source of error and the saturation effects:

$$dV/dt = (\alpha V + S)(1 - V/V_\infty). \tag{3.2}$$

Here α is the rate of growth of the forecast error variance, S the amount of error variance introduced by model deficiencies in one day, and V_∞ is the asymptotic value of the error variance. This equation has the solution

$$V(t) = V_\infty - (V_\infty + S/\alpha)/(1 + \mu), \tag{3.3}$$

where $\mu = C\exp[(\alpha + S/V_\infty)t]$, and the constant $C = (V(0) + S/\alpha)/(V_\infty - V(0))$ is related to the initial value of the error variances.

Preliminary computations were performed allowing $V(0)$ to be different from zero (Kalnay and Dalcher, 1985). It was found that $V(0) \lesssim$

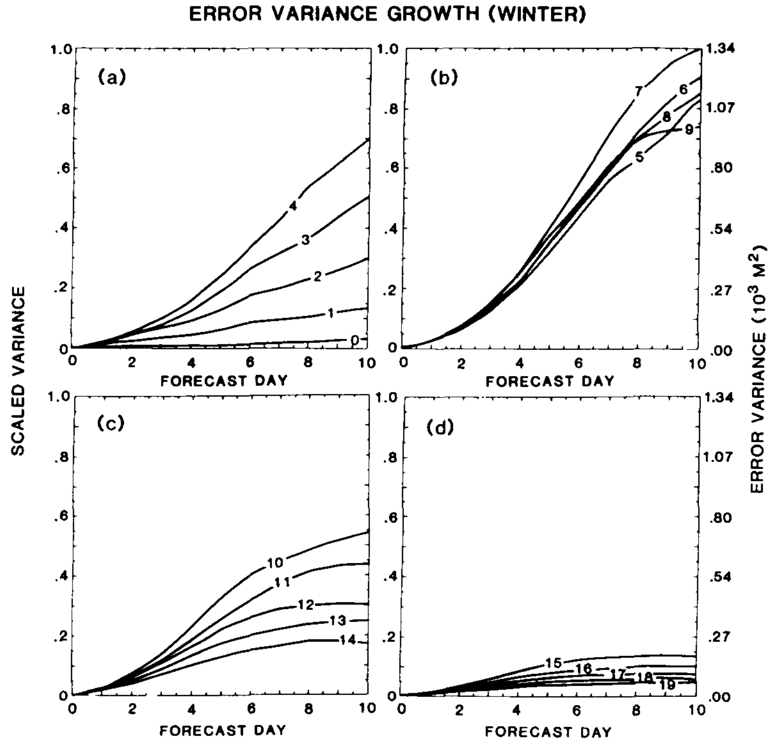

Fig. 7. Error variance growth for waves with total wavenumber $n = 0, 1, \ldots 19$, for the winter.

$0.01 \times V(10$ days), i.e., the extrapolated estimation of the initial error was about $(10\ \text{m})^2$, in basic agreement with current estimates of analysis errors. However, since $V(0)$ is much smaller than both S and V_∞, it is more subjected to sampling fluctuations than the three other parameters. This is especially apparent when the fit is extended to each wavenumber (Section 4), in which case $V(0)$ is rather noisy, oscillating around 2% of the 10-day error variance. For high wavenumbers, which saturate faster and therefore have fewer independent data values, the sampling problem is even worse, and for some wavenumbers, $V(0)$ becomes slightly negative. For this reason we decided to neglect analysis errors. With this assumption $V(0) = 0$ and

$$\mu = S/(\alpha V_\infty) \exp[(\alpha + S/V_\infty)\, t]. \tag{3.4}$$

The solution (3.3) can also be expressed as

$$\begin{aligned} V(t) &= 0.5(V_\infty + S/\alpha) \\ &\quad + \{1 + \tanh 0.5\, [\ln (S/(\alpha V_\infty)) \\ &\quad + (\alpha + S/V_\infty)\, t]\} - S/\alpha. \end{aligned}$$

Fig. 9 shows that this parameterization works remarkably well for both winter and summer when all scales are combined together.

The values of the three parameters are given in Table 1. It is interesting to note that although the error growth rate is similar in the winter and in the summer, the lower value of the asymptotic squared error and the larger external source of error due to model deficiencies combine to produce a significantly faster saturation in the summer than in the winter. The scaled value of the external source of errors, S/V_∞, indicates that from model errors alone, the error variance would reach V_∞ in about 25 days in the winter, and in only about 16 days in the summer.

The shape of the individual error growth for each total wavenumber n suggests that the same parameterization can be applied to each wavenumber (Figs. 7, 8). In Fig. 10 we apply the same function to four individual wavenumbers n, extrapolating it to 30 forecast days. It also shows an excellent fit, and clearly indicates that the

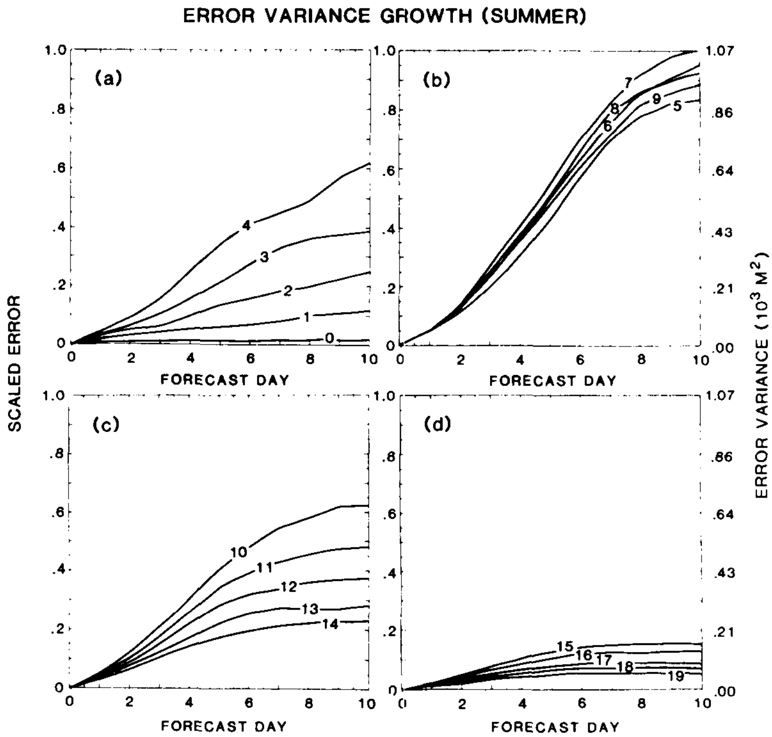

Fig. 8. Same as Fig. 7 but for the summer.

Table 1. *Derived parameters for the global error growth*

	Winter	Summer
V_∞	11076 m^2 $\simeq$ (105 m)^2	9856 m^2 $\simeq$ (99 m)^2
α	0.43 day^{-1}	0.44 day^{-1}
S	439 m^2 day^{-1} $\simeq$ (21 m)^2 day^{-1}	597 m^2 day^{-1} $\simeq$ (24 m)^2 day^{-1}
S/V_∞	0.04 day^{-1}	0.06 day^{-1}

saturation error is attained at earlier times for shorter scales.

4. Internal and external error growth

We next attempt to apply (3.2) to parameterize both the error variance growth of *real forecasts*, as in the last section, and the *growth of the squared differences between forecasts verifying on the same day*. We separate the growth of the difference between two forecasts of length i and j ($i > j$) verifying on the same day t into two stages (Fig. 11): From time $t-i$ to $t-j$, there is real forecast error growth in the first forecast, and we integrate (3.2) assuming $V(t-i) = 0$. Between $t-j$ and t days the two forecasts depart from each other with only internal error growth ("identical twin" experiments). Therefore we apply (3.2) with $S = 0$ and $V(t-j)$ given by the previous solution.

There are now three parameters that are determined in the best fit to the "external" or real

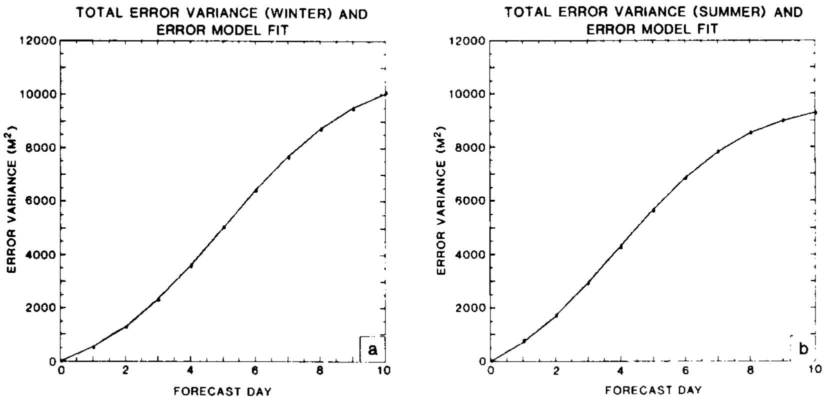

Fig. 9. Total error variance growth. Observed (points) and fitted model (curve): (a) winter; (b) summer.

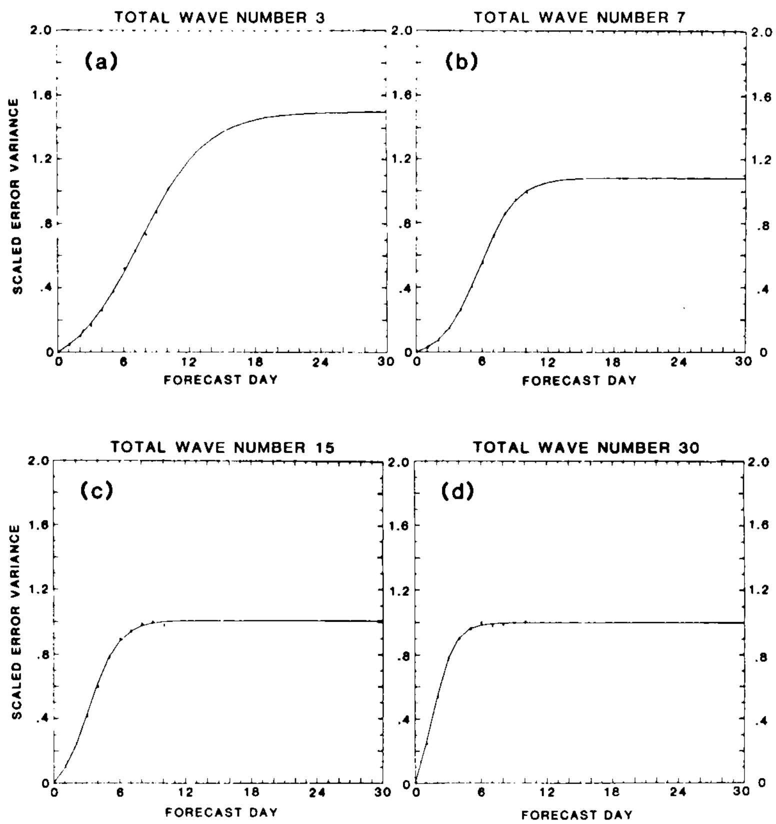

Fig. 10. Winter error variance growth for waves with total wavenumber $n = 3$, 7, and 15. The data values (marked by points) are available for the first 10 days. The error is scaled by its maximum observed value. The fitted function is extrapolated to 30 days: $n = 3$ (a) scaled by 500 $m^2 \approx (22.4\ m)^2$; $n = 7$ (b) scaled by 1255 $m^2 \approx (35.4\ m)^2$; $n = 15$ (c) scaled by 173 $m^2 \approx (13.2\ m)^2$; $n = 30$ (d) scaled by 5.9 $m^2 \approx (2.4\ m)^2$.

forecast errors: V_∞^E, α^E, and S^E. For the forecast differences or "internal" errors we would need to fit 11 parameters: V_∞^I, α^I and the 9 initial values $V_j^I(j)$, $j = 1, 2, \ldots, 9$, for forecasts separated by j days. We have constrained the external and internal errors so that at any day j, $V_j^I(j) = V^E(j)$. These constraints couple the internal and external error growth and reduce the number

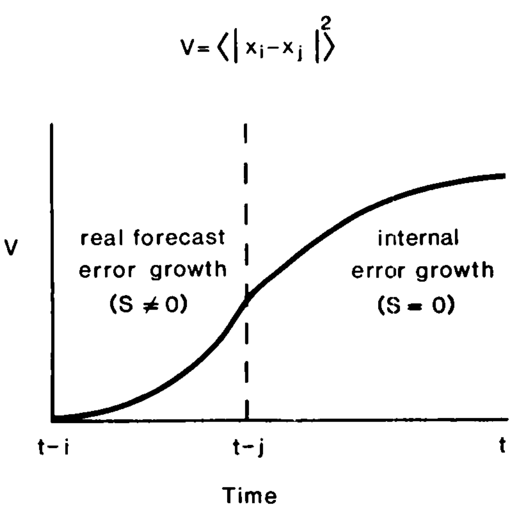

Fig. 11. Schematic of the growth of the squared difference between two forecasts of length i and j ($i > j$) verifying at time t.

of free parameters to five. In addition, we have also assumed that the saturation error energy and the error growth rates are the same for both internal and external errors, thus reducing the total number of parameters to only three. It should be noted that we also tested the fit of the data using different values for the internal and external error growth rate and saturation levels. Even though the data suggests that these values are not identical, the fit was not substantially better, so that the introduction of the extra parameters was not justified.

Fig. 12 presents both the observed (points) and the 3-parameter fir (curves) global squared random differences between i-day and j-day forecasts verifying the same day. Each curve corresponds to a different value of j–i: starting from the bottom the curves correspond to $j - i = 1,2,3,\ldots$. The top curve is the real forecast error variance. The fit in the summer (Fig. 12b) is somewhat poorer than in the winter (Fig. 12a).

The values of the parameters, now derived for both internal and external errors are given in Table 2.

The V_∞ values in Table 2 are virtually identical to the corresponding values in Table 1. The values for α and S/V_∞ are somewhat different. This can be attributed to the fact that there are many more values corresponding to the internal growth. Note that in there is a trade off between α and S: within a certain range an increase in α

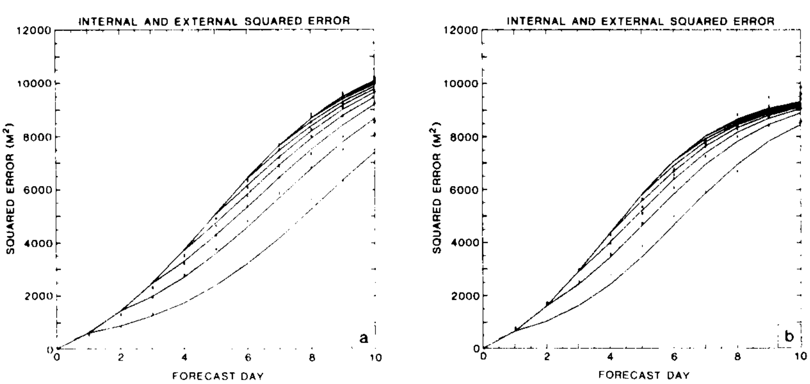

Fig. 12. Global squared random differences between i-day forecast and j-day forecasts verifying on the same day ($i < j$) as a function of j. Each curve corresponds to a different value of $j - i$: starting from the bottom the curves correspond to $j - i = 1, 2, 3, \ldots$. The top curve is the real forecast error. Observed points and model fit (curve) are plotted: (a) Winter; (b) summer.

Table 2. *Derived parameters for the internal and external error growth*

	Winter	Summer
V_∞	$11345\ \text{m}^2 \simeq (106.5\ \text{m})^2$	$9634\ \text{m}^2 = (98.2\ \text{m})^2$
α	$0.39\ \text{day}^{-1}$	$0.51\ \text{day}^{-1}$
S	$508\ \text{m}^2\ \text{day}^{-1} \simeq (22.5\ \text{m})^2\ \text{day}^{-1}$	$521\ \text{m}^2\ \text{day}^{-1} = (22.8\ \text{m})^2\ \text{day}^{-1}$
S/V_∞	0.045	0.054

and a decrease in S will not change the result of the fit substantially, because the term $\alpha V + S$ will not change by much.

It is interesting to compare the results of Lorenz' (1982) parameterization of the growth of the r.m.s. separation between forecasts (eq. 1.1) with our parameterization of internal error variance growth (eq. 3.2 with $S = 0$). The formulations are very similar, except for the fact that we subtracted the systematic error, and, more importantly, that we are parameterizing the growth of the *square* of separation rather than the r.m.s. separation. This results in a significant difference in the "doubling time". Since the squared error quadruples when the r.m.s. error doubles, one would expect that the doubling time t_2 for Lorenz' model will be the same as the quadrupling time τ_4 in our model. However, in the winter case, $t_2 = 2.4$ days (Lorenz, 1982), whereas in our parameterization, using the same forecast/forecast differences as Lorenz did, $\tau_4 = 3.7$ days. This discrepancy is explained by the fact that in both models, the doubling time is not constant (it becomes infinite as $t \to \infty$), and at $t = 0$ it is only estimated by extrapolation to small errors. If we compare Lorenz' scaled model $\mathrm{d}E/\mathrm{d}t = \beta E(1 - E)$ with ours, $\mathrm{d}V/\mathrm{d}t = \alpha V(1 - V)$, and make use of $V = E^2$, we obtain that at any given time $\beta/\alpha = (1 + E)/2$. Since $\tau_4 = \log 4/\alpha$ and $t_2 = \log 2/\beta$ we find that $\tau_4/t_2 = 1 + E$. If the error values used to fit the parameters were vanishingly small, we would indeed obtain $\tau_4 \simeq t_2$; however, the values of the scaled error E available for fitting are mainly in the range 0.4 to 0.8. Therefore it is not surprising that our fit is such that $\tau_4 \sim 1.6\ t_2$. This discussion indicates that the widely used parameter, "doubling time of small errors" is *not a very good measure of error growth.* In practice it cannot be measured directly because the true state of the atmosphere is not known due to analysis errors and problems associated with model initialization. Therefore it can only be determined by extrapolation to small times, and we have shown that the results are very sensitive to the error parameterization. On the other hand, the error growth at finite times is well defined from the available data. Arpe et al. (1985) have also pointed out the difficulty of estimating the doubling time of smaller errors.

We now apply the three-parameter model corresponding to Fig. 11, to each wavenumber n, and derive the main result of this paper, i.e., *the wavenumber dependence of parameters such as error growth, saturation error levels and the dynamical limit of predictability.* In order to reduce fluctuations due to sampling, we smooth the data in total wavenumber domain using a (0.25, 0.5, 0.25) operator, which does not affect the results in any significant way.

The parameters derived for the winter are presented in Fig. 13. Fig. 13a shows the analysis variance, V_{an} which, probably due to sampling fluctuations, has two maxima at $n = 5$ and $n = 7$, and a small peak at $n = 1$. Fig. 13b presents V_∞, the estimated error variance saturation. Like the error variance at day 10 (not shown), it has a single peak at $n = 7$. The ratio of V_∞/V_{an}, (not shown) oscillates about 1.8, except for $n = 1$ where it is 0.6. It is not surprising that this ratio is less than 2, because the analysis variance contains a component due to the seasonal cycle, due to the fact that we have defined "climatology" as the 100-day average. The seasonal cycle is also present in the forecasts, and therefore, it is essentially excluded from the error variance.

In Fig. 13c, we present the ratio between V_∞ and $V_{\max}$, the maximum observed error variance which generally occurs at 10 days. It is larger than one for $n \leqslant 10$, indicating that the model has not reached saturation by day 10, and for the planetary waves the saturation error vari-

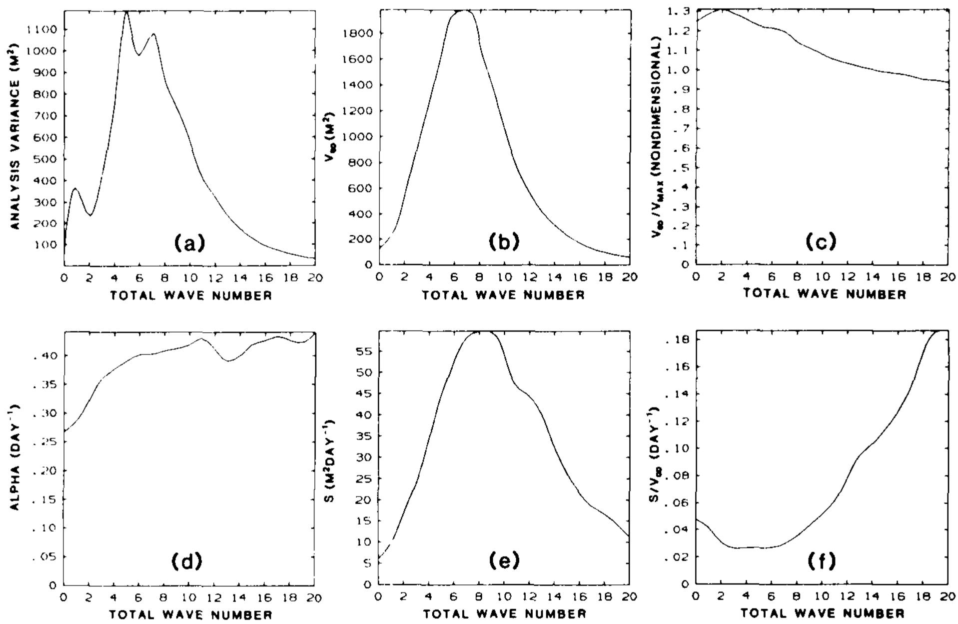

Fig. 13. Fitted parameters (three-parameter model) as a function of total wave number for the winter. (a) Analysis variance; (b) V_∞, the saturation error variance; (c) V_∞ divided by $V(10)$, the error variance at day 10; (d) error growth rate; (e) S, the source of errors due to model deficiencies (f) S/V_∞.

ance is about 30% larger than the error at day 10. The values of $V_\infty/V_{\max}$ slightly smaller than one at high wavenumbers are due to our assumption that the internal saturation error variance V_∞^{I} is equal to the external value V_∞^{E} whereas the data indicates that for high wavenumbers, $V_\infty^{\mathrm{I}} < V_\infty^{\mathrm{E}}$.

Fig. 13d presents the error variance growth rate α, which increases with wavenumber from about 0.3 day^{-1} for $n = 1$ to more than 0.40 day^{-1} for $n = 10$ and larger. Fig. 13c presents S, the source of squared errors due to model deficiencies. S varies from about (3 m)^2/day at short and longwaves, to a maximum of about (7.5 m)^2/day for $n = 8$. In order to display the relative importance of model errors, we divide S by V_∞. Fig. 13f indicates that at longwaves, model errors alone without internal error growth would produce saturation in about 30 days. For $n \gtrsim 6$, this time decreases monotonically with wavelength, until it becomes as short as 5 days at $n \sim 20$. The scaled model source of error may tend to increase monotonically with wavenumber because of the use of second-order finite differences in the 1980/81 ECMWF model. It should be interesting to re-evaluate this quantity with the current ECMWF spectral model (Arpe and Klinker, 1986).

The corresponding results for the NH summer are presented in Fig. 14. The parameters and their distribution with wavenumber are generally similar to those in the winter. The main difference are that the variances are smaller by about 2/3, the error growth is somewhat larger, from 0.30 day^{-1} at $n = 1$ to about 0.50 day^{-1} for $n \geqslant 8$, and that long waves are close to saturation after 10 days with V_∞ only about 10% larger than $V(10)$. All these differences point to less predictive skill in the June–August 1981 period than in the December 1980–March 1981 season. Since the results presented are global it is clear that the NH summer characteristics dominate the global circulation.

It is of great interest to derive *the limit of dynamic predictability*, which we define as the time $t_{0.95}$ at which error reaches 95% of its saturation level. The reason we have adopted this definition is that as long as the forecast error

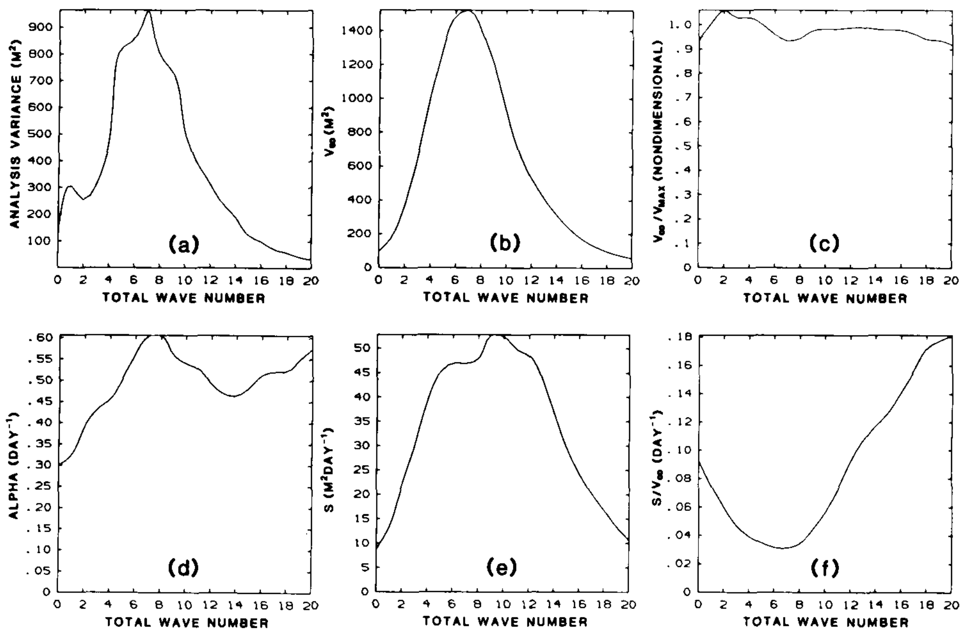

Fig. 14. Same as Figure 13 but for the summer.

variance has not saturated, i.e., reached twice the value of climatological error variance, a statistical combination of the forecast and climatology has a smaller error than climatology. Fig. 15a presents the winter limit of dynamic predictability for both the real model errors and for a model with internal errors only. The real model error curve, which is obtained by fitting the observed error data, shows that for low wavenumbers ($n \lesssim 10$), there is still predictability in the ECMWF model after 10 days, whereas higher wavenumbers become saturated at increasingly shorter times. The curve corresponding to a perfect model with only internal errors, is derived using (3.2) with $S = 0$ and starting from the 6-h interpolated errors. This level of error was chosen as representative of the present level of analysis error (about 12 m). The result suggests that with a perfect model and the same error growth rate, predictability would be about a week longer, reaching more than 2 weeks in the winter.

The limit of predictability for the summer (Fig. 15b) is, as expected from the previous results, considerably shorter. Even for a perfect model, predictability reaches 2 weeks only for $n \leqslant 6$.

In Figs. 16a and b we determine the time, $t_{0.5}$, at which the errors cross 50% of the saturation value, i.e., the time at which the mean squared errors of a dynamical forecast become larger than those of climatology. At this time, a purely statistical forecast becomes better than a purely dynamical one. Of course, a statistical-dynamical forecast will be more accurate than either the dynamical or the statistical prediction throughout the length of the forecast. The 50% error level is reached for short waves at about 2 days. For long waves, it is about 6 days in the winter and 4 days in the summer.

When all the scales are combined together, the limit of predictability ($t_{0.95}$) with the current model is 12.0 days in the winter and 9.4 days in the summer. For a perfect model with the same error growth these limits would be 20.0 and 15.1 days respectively. The 50% error level is reached at 5.5 days in the winter and 4.3 days in the summer.

5. Conclusions

We have studied the forecast error growth in the 100-day ECMWF data set of 10 days fore-

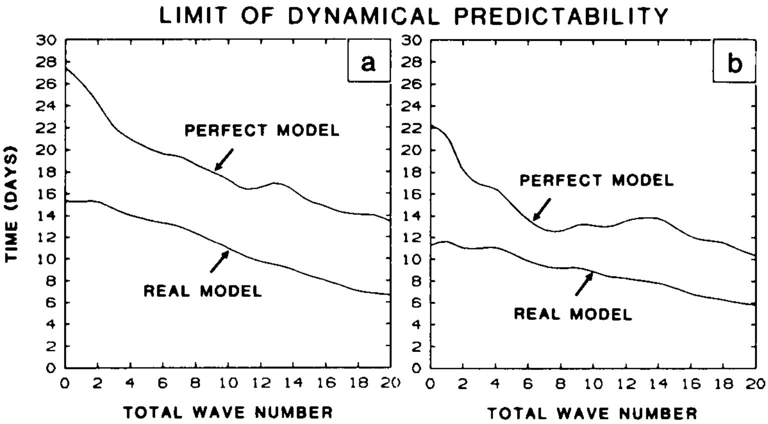

Fig. 15. Limit of dynamic predictability defined as the time at which for forecast error reaches 95% of the errror saturation value. The lower curve corresponds to the current model, and the upper curve to a perfect model. (a) Winter, (b) summer.

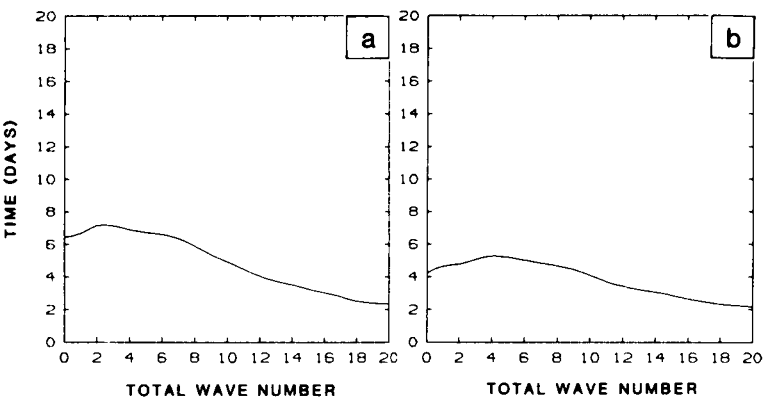

Fig. 16. Time at which the squared errors of the present model reach 50% of saturation and become larger than the errors of climatology. (a) Winter, (b) summer.

casts previously utilized by Lorenz (1982), separating the square of the error into systematic and random components.

The spectral distribution of the systematic and random errors is very different. The systematic error is dominated by a few wave components of planetary scale. The random error variance occurs with an approximate equiparition of energy between all zonal wavenumbers m corresponding to the same total wavenumber n except that energy decreases rapidly as $m \to n$. Based on this result, we combine the random error variance for all zonal wavenumbers and study its dependence on total (2-dimensional) rather than zonal wavenumber.

We extend Lorenz (1982) model for global r.m.s. error growth by allowing for the effect of errors associated with deficiencies in the forecast model, and apply this new parameterization to the error variance of 10-day ECMWF operational forecasts. The fit to the real forecast errors is excellent, and the fit to the differences between forecasts is moderately good. We point out that the commonly used parameter "doubling time of small errors" is *not* a good measure of error growth. It can only be determined by extrapolation to small errors, and it is very sensitive to the method of extrapolation. Error growth at finite times is a better parameter because it is well defined by the data.

We next fit the same three-parameter model to both real forecast errors and forecast differences separately for each total wavenumber n. The dependence of these parameters on n constitutes the main result of the paper. Preliminary computations including a fourth parameter $V(0)$, the initial error variance derived by extrapolation to the initial time, indicated that $V(0)$ is about 1–3% of the error variance at 10 days or about $(10 \text{ m})^2$. However, because of its smallness, $V(0)$ is very subjected to sampling fluctuations, so that we choose to neglect analysis errors and assume $V(0) = 0$.

The error growth rate α increases almost monotonically with wavenumber, from about 0.3 day^{-1} at long waves to about 0.45 day^{-1} at medium and short waves. The saturation error variance V_∞ is similar to the error variance at 10 days, except for longwaves where V_∞ is larger than $V(10)$. Waves with $n < 10$ have not reached saturation at day 10 in the winter forecasts. The source of external error due to model deficiencies S, has a peak at $n \cong 7$ like V_∞ and the analysis variance. However, the scaled source of errors S/V_∞ increases monotonically with wavenumber from about 3% day^{-1} at low wavenumbers to about 20% day^{-1} at high wavenumbers. The operational model used during 1980/81 had second order finite model differences at ECMWF. It would be interesting to see whether the strong dependence of S/V_∞ on wavenumber is still present in the current spectral model.

The 50% level of errors, when the dynamical forecast mean squared when errors become equal to those of climatology, is reached at 2 days for short waves and 4-6 days for long waves. Although a statistical-dynamical forecast is more accurate than a purely dynamical forecast throughout the length of the forecast, at this time it becomes essential to statistically combine the dynamical forecast with climatology.

Finally, we estimate the theoretical limit of dynamical predictability as a function of horizontal wavenumber. We define it as the time at which the error variance reaches 95% of the saturation value. This time decreases monotonically with n. In the winter, waves with $n \lesssim 10$ have not yet reached 95% of saturation at 10 days. In a perfect model with error growth similar to the present model the predictability would be extended by 2 or 3 days. In the summer, error growth rates and model deficiencies are larger than in winter, and the saturation error variance smaller. The limit of predictability in close to 10 days even for long waves.

6. Acknowledgements

We are very grateful to a reviewer, Dr. C. Leith, who suggested modifications of the manuscript which resulted in major improvements of the presentation of results. We had useful discussions with Drs. R. N. Hoffman, D. Reuter and R. Livezey. The manuscript was typed by Benita Richardson and Mary Ann Wells, and Laura Rumberg expertly drafted the figures. The data sets were kindly provided by ECMWF.

REFERENCES

Arpe, K., Hollingsworth, A., Tracton, M. S., Lorenc, A. C., Uppala, S. and Kållberg, P. 1985. The response of numerical weather prediction systems to FGGE level IIb data—Part II: Forecast verification and implications for predictability. *Q. J. R. Meteorol. Soc. 111*, 67–101.

Arpe, K. and Klinker, E. 1986. Systematic errors of the ECMWF operational forecasting model in mid-latitudes. *Q. J. R. Meteorol. Soc. 112*, 181–202.

Bengtsson, L. 1985. Medium-Range Forecasting—The Experience of ECMWF. *Bull. Am. Meteorol. Soc. 66*, 1133–1146.

Boer, G. J. 1984. A spectral analysis of the predictability and error in an operational forecast system. *Mon. Weather Rev. 112*, 1183–1197.

Charney, J. G., Fleagle, R. G., Riehl, H., Lally, V. E. and Wark, D. Q. 1966. The feasibility of a global observation and analysis experiment. *Bull. Am. Meteorol. Soc. 47*, 200–220.

Dalcher, A., Kalnay, E. and Hoffman, R. N. 1985. Application of the lagged average forecast method to ECMWF 10-day forecasts. Preprints from the *Ninth Amer. Meteor. Soc. Conference on Probability and*

Statistics in Atmospheric Sciences. Virginia Beach, VA., October 1985, 130–136.

Hoffman, R. N. and Kalnay, E. 1983. Lagged average forecasting an alternative to Monte Carlo forecasting, *Tellus 35A*, 100–118.

Hoffman, R. N. and Kalnay, E. 1984. Lagged average forecasting, some operational considerations. *Predictability of fluid motions, American Inst. of Phys. Conf. Proc.*, G. Holloway and B. J. West, editors, *106*, 141–147.

Kalnay, E. and Dalcher, A. 1985. Error growth in operational ECMWF Forecasts Preprints from the *Seventh Conference on Numerical Weather Prediction*. Montreal, P. Q., Canada, June 1985, pp. 183–189.

Leith, C. E. 1978. Objective methods for weather prediction, *Ann. Rev. Fluid Mech. 10*, 107–128.

Leith, C. E. 1982. Statistical methods for the verification of long and short range forecast. *European Centre for Medium Range Weather Forecasts, Seminar 1981, Problems and Prospects in Long and Medium Range weather Forecasting*, 14–18 September, 313–333.

Lorenz, E. N. 1965. A study of the predictability of a 28-variable atmospheric model. *Tellus 17*, 321–333.

Lorenz, E. N. 1982. Atmospheric Predictability experiments with a large numerical model. *Tellus 34*, 505–513.

Savijärvi, H. 1984. Spectral properties of analyzed and forecast global 500 mb fields. *J. Atmos. Sci. 41*, 1745–1754.

Shukla, J. 1981. Dynamical predictability of monthly means. *J. Atmos. Sci. 38*, 2547–2572.

Smagorinsky, J. 1969. Problems and promises of deterministic extended range forecasting. *Bull. Am. Meteorol. Soc. 50*, 286–311.

Wallace, J. M., Tibaldi, S. & Simmons, A. J. 1983. Reduction of systematic forecast errors in the ECMWF model through the introduction of an envelope orography. *Q. J. R. Meteorol. Soc. 109*, 683–717.